Materials Science and Engineering, 77 (1986) 199-212

Effect of Microstructure on Reliability Predictions for Glass Ceramics

R. F. COOK*, S. W. FREIMAN and T. L. BAKER

Inorganic Materials Division, National Bureau of Standards, Gaithersburg, MD 20899 (U.S.A.)

(Received February 27, 1985)

ABSTRACT

A study is made of the fracture properties of a range of three Li_2O-SiO_2 glass ceramics with different grain sizes. Both equilibrium and kinetic crack propagation parameters are evaluated using the controlled flaw indentation technique with a view to making reliability predictions. Fracture toughness in the well-behaved large-contact-flaw range is found to increase with increasing grain size. At low contact loads the strength and apparent toughness are found to fall below the predictions of the well-behaved region, this tendency increasing with increasing grain size. At the fixed contact load chosen for fatigue testing, the susceptibilities to slow crack growth for the three materials are found to be similar. A theory is developed to allow the variations in apparent toughness to be taken into account for lifetime prediction. The results suggest that caution must be exercised when reliability predictions are made for materials showing the effects of crack-microstructure interaction, especially in extrapolations to low contact loads.

1. INTRODUCTION

Environmentally enhanced crack growth occurs in almost all ceramics which are of interest for structural applications and hence there always exists a possibility of in-service failure. In order to prevent such failures it is necessary to establish stress levels at which components can be safely used within their desired service life so that the extent of crack growth within this period will not lead to failure. The accuracy of such predictions is dependent on the accuracy with which we can measure the fracture parameters for the material and material-environment system. The most important of these are the fracture toughness (characterizing equilibrium fracture) and the susceptibility to environmental slow crack growth (characterizing kinetic fracture). Hence, choosing a ceramic material for a structural application involves the relationship between the ceramic microstructure and the crack propagation properties.

Much recent work has been directed towards understanding the influence of microstructure on crack propagation and usually examines the effects of microstructure on the observed component strength and/or material fracture toughness. Little work has been done to examine kinetic crack growth as a function of microstructural scale or as a crack propagates through the microstructure.

The objective of this study was to measure the equilibrium and kinetic crack growth parameters for an Li_2O-SiO_2 glass ceramic heat treated to yield three different microstructures. Specifically, the aims were to determine unambiguously the effects of microstructure on the fracture parameters, providing a basis for the development of crack-microstructure models and to make reliability predictions based on these data to aid in materials selection. Measurements were made using the controlled indentation flaw technique. In this technique a dominant flaw of controlled size and nature is introduced into a specimen surface and strength testing of the specimen carried out under controlled conditions. Explicit and well-verified models allow the results obtained to be related unambiguously to the intrinsic material properties. Equally important for this study was the advantage of controlling the size of the dominant flaw relative to that of the microstructure.

*On leave from the University of New South Wales, New South Wales, Australia.

0025-5416/86/$3.50

2. BACKGROUND THEORY

Most of the theory used to relate the observed strengths and indentation contact and crack length dimensions to the intrinsic material properties has been described extensively elsewhere and hence only the relevant results will be given here [1–8].

2.1. *Stress intensity factor*

The total stress intensity factor* K on an indentation crack of length c under an applied stress is given by

$$K = \psi \sigma_a c^{1/2} + \frac{\chi P}{c^{3/2}} \tag{1}$$

where σ_a is the applied stress, P the indentation load used to produce the flaw, ψ a geometrical constant (about 1.44) and χ a material indenter constant. The first term on the right-hand side of the equation arises from the applied stress, and the second arises from the mismatch of the elastic–plastic deformation surrounding the indentation [1, 2]. The presence of other stresses on the crack, such as those due to microstructural interactions, appears in the analysis as third or further terms on the right-hand side of eqn. (1).

2.2. *Indentation crack lengths*

Immediately after indentation the crack length is in equilibrium with the residual stress arising from the elastic–plastic mismatch and thus we may write for this crack length c_0 ($\sigma_a = 0$);

$$K_c = \frac{\chi P}{{c_0}^{3/2}}$$

where K_c is the equilibrium stress intensity factor or fracture toughness. Hence by measuring the quantity $P/{c_0}^{3/2}$ the fracture toughness may be calculated, provided that the constant χ is known. Workers have shown that χ may be represented by

$$\chi = \xi \left(\frac{E}{H}\right)^{1/2}$$

where E is Young's modulus, H the hardness and ξ a material-independent constant† approximately equal to 0.016 [2, 3]. However, unless strict precautions are taken, c_0 is very difficult to measure; moisture-assisted slow crack growth increases c_0 to c_0' under the influence of the residual stress. The presence of secondary crack systems (*e.g.* laterals) can reduce χ below its original level, further complicating the system. Empirically, however, it is found that

$$K_c = \xi' \left(\frac{E}{H}\right)^{1/2} \frac{P}{(c_0')^{3/2}} \tag{2}$$

allowing K_c to be estimated from the post-indentation crack lengths, given a value of ξ' [6].

2.3. *Inert strengths*

Equilibrium crack growth ($K = K_c$) under the action of an applied stress is obtained by testing in an inert environment. By inserting the equilibrium condition $K = K_c$ into eqn. (1) and requiring the equilibrium to be critical ($dK/dc = 0$), the critical stress and crack length are defined:

$$\sigma_m = \frac{3K_c}{4\psi {c_m}^{1/2}} \tag{3a}$$

$$c_m = \left(\frac{4\chi P}{K_c}\right)^{3/2} \tag{3b}$$

The combination of these two equations and the use of the explicit form of χ lead to

$$K_c = \eta \left(\frac{E}{H}\right)^{1/8} (\sigma_m P^{1/3})^{3/4} \tag{4}$$

where η is a material-independent constant approximately equal to 0.65 [4, 6]. Two aspects of eqn. (4) should be noted: firstly, if eqn. (1) holds for the material, then $\sigma_m P^{1/3}$ should be a constant independent of P; secondly, the fracture toughness may be estimated from inert strength measurements (provided that $c_0' \leqslant c_m$).

*As we consider only mode I crack propagation here the subscript I was not added to K.

†Recent results suggest that the deformation process in glasses is sufficiently different from that in polycrystalline ceramics that significant variations in ξ are produced [5].

2.4. Fatigue strengths

Non-equilibrium or kinetic crack growth under the action of an applied stress is obtained by testing in the presence of a chemically active environment (usually water). In these cases, crack extension occurs at stress intensities less than K_c and the crack velocity v can be shown empirically to follow the power law approximation:

$$v = v_0\left(\frac{K}{K_c}\right)^n \tag{5}$$

where v_0 and n are material–environment constants. The most practical method of examining the effects of slow crack growth on strength and determining the fatigue constants (particularly n) is by dynamic fatigue, where $\sigma_a = \dot{\sigma}_a t$ and the applied stress rate $\dot{\sigma}_a$ is a constant. By combining eqns. (1) and (5) and imposing the dynamic fatigue condition the resulting differential equation may be solved to give the dynamic fatigue strength σ_f (the applied stress at failure) as a function of the applied stress rate [7, 8]:

$$\sigma_f = (\lambda' \dot{\sigma}_a)^{1/(n'+1)} \tag{6}$$

where the intrinsic material–environment parameters are related to the apparent fatigue parameters n' and λ' by [8]

$$n = \frac{4n'}{3} - \frac{2}{3} \tag{7}$$

$$v_0 = \frac{\sigma_m{}^{n'} c_m (2\pi n')^{1/2}}{\lambda'} \tag{8}$$

Thus, by measuring the failure strength of indented specimens as a function of the applied stress rate and performing regressions on the data obtained, the apparent kinetic parameters n' and λ' are determined. Usage of eqns. (7) and (8) then allows the calculation of the intrinsic material–environment parameters. (The transformation equations, eqns. (7) and (8), also only apply for $c_0' \leqslant c_m$.) The parameters n' and λ' are used for lifetime prediction and discussion of this will be left until Section 6.

3. EXPERIMENTAL DETAILS

3.1. Materials

The materials investigated were three glass compositions, heat treated to yield three different microstructures designated as S(396), SP(398) and SP2(405) (Sandia National Laboratories) (the nominal compositions are given in Table 1). Figure 1 shows micrographs of the polished surfaces of the three materials; a two-phase structure is immediately apparent. The minor phase particles take the form of plates and have been identified as Li_2SiO_3, the major phase is predominantly cristobalite with some remaining amorphous SiO_2 [9]. The size of the minor phase grains and the mean free path in the major phase increases in the order SP(398), S(396), SP2(405), while the volume fraction of the minor phase decreases in this order (Table 2). The mean free path λ in the matrix was measured using the technique described by Freiman [10]:

$$\lambda = \frac{1 - V_f}{N_L}$$

where V_f is the volume fraction of the minor phase and N_L the number of intersections per unit length of line in the composite. The parameters V_f and N_L were averaged from five representative polished areas on each material.

The materials were received as plates which were diamond sawed and ground down to 600 grit SiC into test bars (3.5 mm × 5.5 mm × 100 mm). All but a few of the bars were annealed at 600 °C for 30 min and allowed to furnace cool to remove possible stresses introduced by machining [11]. The remaining specimens were diamond polished to the 1–3 μm level; these were used for microstructural examination and indentation crack length measurement as well as to confirm the fact that in strength tests the annealing procedure had removed the machining-induced stresses.

TABLE 1

Glass compositions

Material	*Amount* (wt.%) *of following compounds*					
	SiO_2	Li_2O	B_2O_3	K_2O	P_2O_5	Al_2O_3
S(396)	71.7	12.6	3.2	4.9	2.5	5.1
SP(398)	69.7	12.6	3.2	4.9	4.5	5.1
SP2(405)	72.7	12.6	3.2	4.9	1.5	5.1

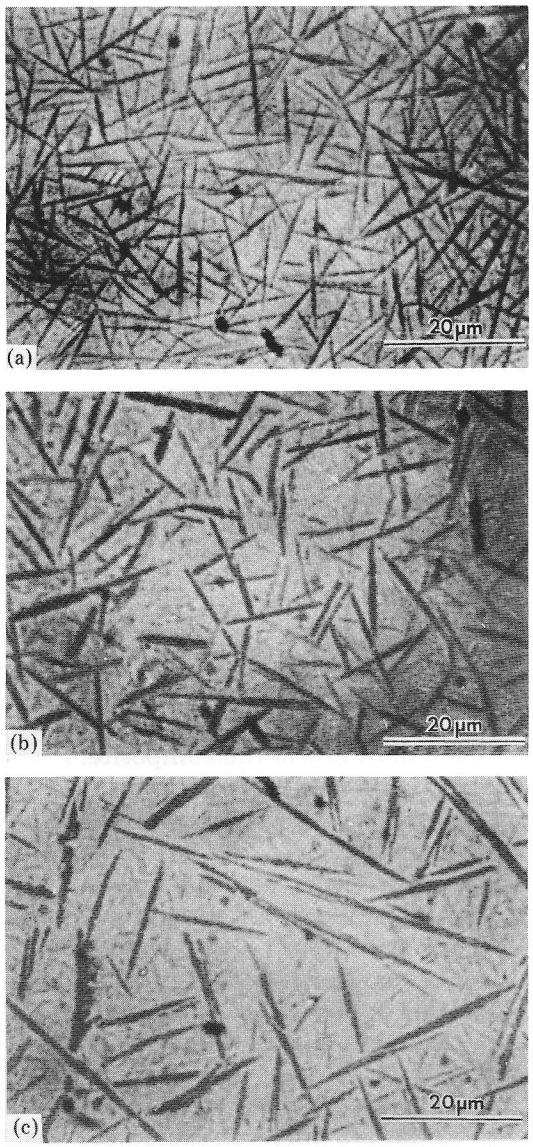

Fig. 1. Optical micrographs of the polished (1 μm) surfaces of the three glass ceramics (a) SP(398), (b) S(396) and (c) SP2(405) (cross-polarized light). Contrast arises because the minor phase preferentially wears during the polishing process.

TABLE 2

Microstructural details

Material	*Minor phase*		*Major phase, mean free path* λ (μm)
	Particle dimensions (μm)	*Volume fraction* V_f	
SP(398)	17 × 1.5	0.33	1.19
S(396)	20 × 2	0.22	1.90
SP2(405)	41 × 3.4	0.20	2.30

Specimens for strength testing were edge bevelled (about 0.25 mm radius) before annealing to remove spurious large edge flaws which might prevent the ensuing indentation crack from becoming the dominant flaw. The bevelling prevented the loss of data from edge failures and the consequent biasing of the indentation failure data, particularly at low indentation loads where microstructural effects might be expected to dominate.

3.2. Indentation measurements

Six to eight Vickers indentations were made on the polished surfaces of each material in air at indentation loads from 3 to 50 N using a standard hardness test machine (Zwick International). The lengths of the diagonals of the resulting square impressions and the lengths of the cracks emanating from the impression corners were then measured optically. Crack length measurements were made approximately 20 min after indentation, during which time the specimens were in ambient air.

3.3. Strength tests

Specimens for inert strength tests were indented in the center of the prospective test face with loads in the range 2–200 N and broken in a completely flexible four-point bend jig with an inner span of 7.5 mm and an outer span of 23 mm at a stressing rate of between 6 and 7 GPa s^{-1}. Before testing, a drop of silicone oil was applied to the test surface to exclude the presence of atmospheric moisture. Fracture occurred in less than 30 ms; loads were monitored with a piezoelectric load transducer. Checks on the annealing procedure were made by measuring the inert strengths of polished unannealed specimens indented at loads of 2–100 N. No significant differences were observed between the strength of the annealed specimens and the strength of the polished unannealed specimens, indicating that the annealing procedure was satisfactory.

Specimens for fatigue strength tests were indented in the center of the test face with a load of 10 N and broken in distilled water in the four-point bend apparatus. Six stressing rates were used, spread over five orders of magnitude; for the slower tests (a failure time greater than 10 s) a standard resistance

strain gauge load cell was used to monitor the breaking load. The fracture surfaces of all strength specimens were inspected optically to ensure that failure had occurred from the indentation flaw. Stresses were calculated from simple beam theory.

3.4. Instability of crack length measurements

In order to determine the quantity c_m necessary for fatigue parameter calculation and to ensure that some stable crack growth had occurred from c_0' to c_m during the inert strength tests, measurements were made of the critical crack dimensions using the "dummy" technique [5]: three indentations were made 1.5 mm apart in the center of the test face of polished specimens at indentation loads of 2–100 N. The specimens were then broken in dry N_2 gas at 6–7 GPa s^{-1}. Failure occurred from one of the indentations while at the remaining two intact dummy indentations the cracks perpendicular to the applied stress had grown from c_0' to c_m. Optical microscope measurements were made of these indentations. In all cases, some crack growth was observed.

4. RESULTS

4.1. Indentation crack lengths

Figure 2 presents the indentation parameters $P/(c_0')^{3/2}$ and the hardness ($H = P/2a^2$ where $2a$ is the impression diagonal length) as a function of indentation load. The parameter $P/(c_0')^{3/2}$, which is proportional to K_c, increases with increasing grain size (in the order SP(398), S(396), SP2(405)) as does, to a smaller extent, the hardness. The hardness decreases slightly with increasing indentation load, a phenomenon observed in other materials, while the parameter $P/(c_0')^{3/2}$ remains relatively constant.

4.2. Inert strength measurements

Figure 3 shows the inert strengths σ_m of the three materials as a function of indentation load P. As can be seen, there are marked deviations from the $P^{-1/3}$ behavior predicted by eqn. (4) (full line). The strengths fall below the $P^{-1/3}$ line at low indentation loads, this tendency increasing with increasing grain size. The strong deviation from the expected behavior which has been observed in many other materials [4, 12] indicates that the driving force in eqn. (1) is in error at low indentation loads. However, we may regard the quantity $\sigma_m P^{1/3}$ as proportional to the "effective" fracture toughness K_c^{eff}. Figure 4 shows the quantity K_c^{eff} calculated from eqn. (4) as a function of indentation load for three materials. The general increase in K_c^{eff} with P is obvious for all three materials (equivalent to deviations from the $P^{-1/3}$ line in Fig. 3). The departure from a constant

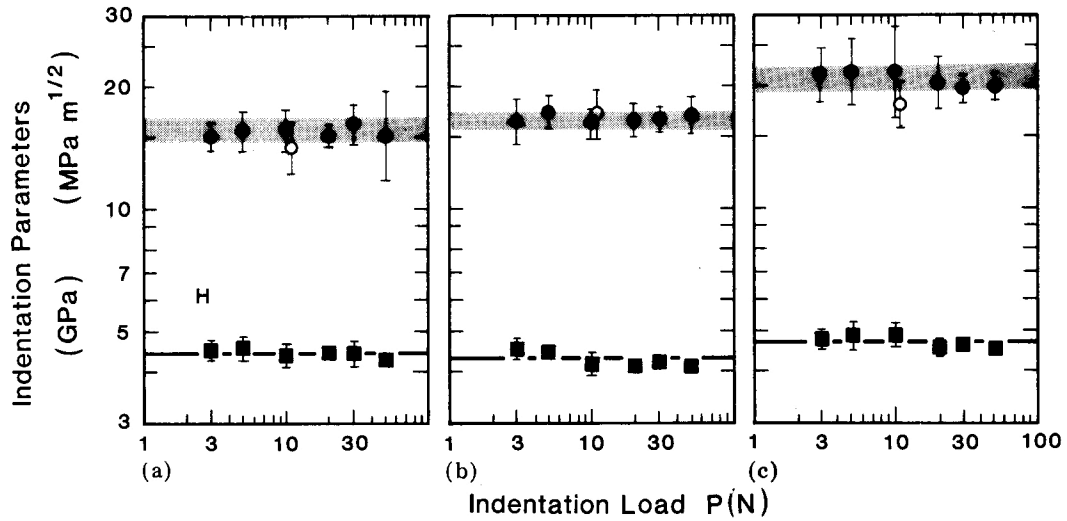

Fig. 2. Indentation parameters $P/(c_0')^{3/2}$ as a function of indentation load for the three glass ceramics (a) SP(398), (b) S(396) and (c) SP2(405): ●, ■, mean and standard deviation of measurements made on six to eight indentations; ○, from measurements made on specimens used in c_m determinations; the shaded bands represent the mean and standard deviation over all measurements for a given material.

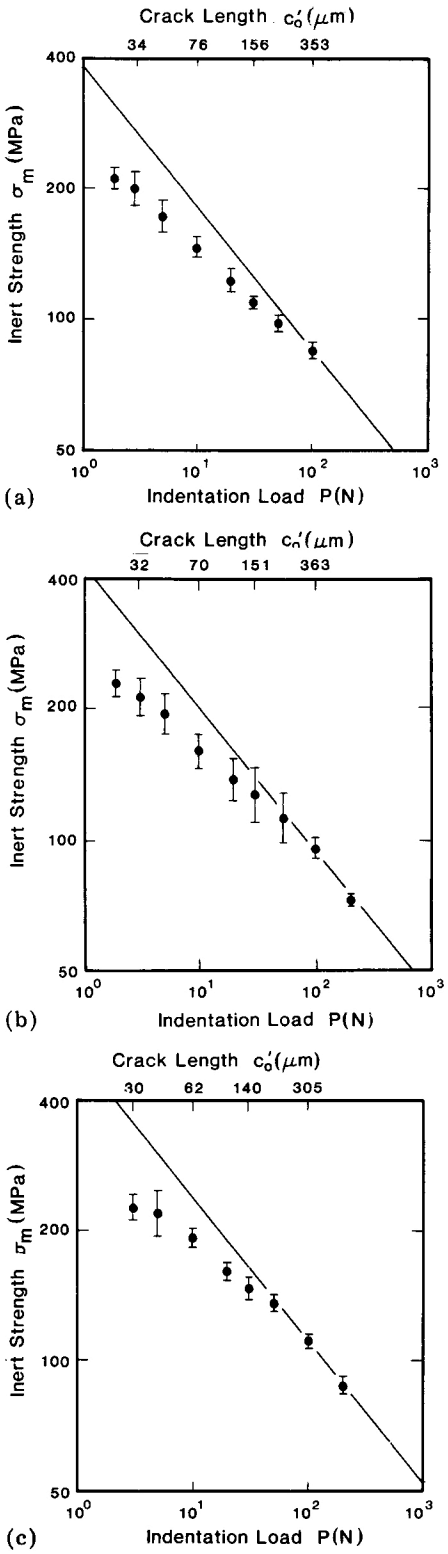

Fig. 3. Strength degradation plots for the three materials (a) SP(398), (b) S(396) and (c) SP2(405): ●, mean and standard deviations of approximately 12 inert strength measurements at each indentation load; ——, expected $P^{-1/3}$ dependence predicted from the assumed "well-behaved" $P \geqslant 100$ N data.

value of K_c^{eff} can also be seen to increase with increasing grain size, consistent with Fig. 3. At large indentation loads, K_c^{eff} appears to reach a plateau and we might regard this level as representing the "true" polycrystalline fracture toughness of the material as would be measured by macroscopic (large-crack) techniques (such as the double-cantilever-beam method). This plateau level of toughness can be seen to increase with increasing grain size as does the average over the range of flaw sizes tested, a trend noted previously in the indentation crack length measurements. Table 3 shows the toughness values calculated from the $\sigma_m P^{1/3}$ data in the well-behaved large-P region compared with those for soda–lime glass and Pyroceram C9606 and, at an indentation load of 10 N, the value chosen for the dynamic fatigue studies.

In view of the strong variations in $\sigma_m P^{1/3}$ seen at low P it is interesting to consider the lack of variation seen in the $P/(c_0')^{3/2}$ parameter (Fig. 2). Diminution of variation in this parameter compared with the strength parameter has been observed in other materials displaying similar apparent microstructural effects [6]. The most likely reason for this discrepancy is that the free surface may to some extent relax the effects associated with the microstructure, thus reducing any third term in the stress intensity relation to negligible proportions at the surface.

The parameter $\sigma_m c_m^{1/2}$ determined from inert strength tests on specimens containing dummy indentations can also be used to determine the effective toughness [5]. Trends in the toughness determined from this parameter with indentation load for a given material and between materials with increasing grain size were similar to those shown in Fig. 4. K_c values determined from fracture surface analyses [9] are also in good agreement with those obtained from the c_m measurements on the tensile surface. Table 3 shows the toughness calculated from the hybrid technique for the $P = 10$ N data. Tentative evidence is provided by the toughness values determined from the $\sigma_m P^{1/3}$ and $\sigma_m c_m^{1/2}$ data as to the mode of deformation. A recent paper has indicated that large discrepancies may occur between K_c values calculated by the strength and hybrid methods if there is appreciable anomalous deformation associated

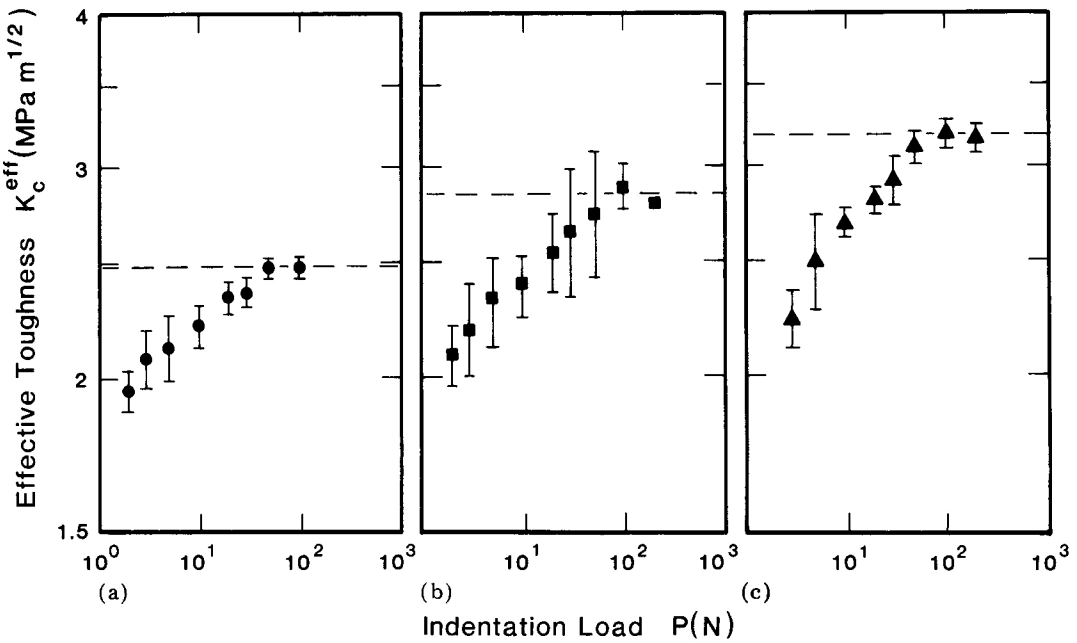

Fig. 4. Effective toughness K_c^{eff} as a function of indentation load for the three materials (a) SP(398), (b) S(396) and (c) SP2(405): data taken from Fig 3; ——, limiting toughness obtained at large flaw sizes, which increases with increasing grain size. The general increase in the average (and spread) of this parameter with increasing grain size should be noted.

TABLE 3

Hardness and fracture toughness data

Material	*H* (GPa)	K_c[a] (MPa m$^{1/2}$)		
		(1)	*(2)*	*(3)*
SP(398)	4.4 ± 0.1	2.47 ± 0.05	2.22 ± 0.09	2.2 ± 0.2
S(396)	4.3 ± 0.07	2.84 ± 0.07	2.40 ± 0.14	2.3 ± 0.3
SP2(405)	4.8 ± 0.1	3.18 ± 0.09	2.70 ± 0.07	2.9 ± 0.4
Soda-lime glass	6.6	1.11	1.10 ± 0.06	0.78 ± 0.05
Pyroceram C9606	8.4	2.51	2.51 ± 0.08	2.3 ± 0.2

[a](1), $K_c = \eta(E/H)^{1/8}(\sigma_m P^{1/3})^{3/4}$, $\eta = 0.65$, $P \geqslant 100$ N; (2), $K_c = \eta(E/H)^{1/8}(\sigma_m P^{1/3})^{3/4}$, $\eta = 0.65$, $P = 10$ N; (3), $K_c = 2.02(\sigma_m c_m^{1/2}) - 0.68$, $P = 10$ N.

with the indentation contact [5]. The data in Table 3, columns (2) and (3), show that these values of the toughness at $P = 10$ N are in good agreement for the glass ceramics, suggesting that the deformation associated with contact events in these materials as well as in the other glass ceramic considered is largely volume conserving (compare the values for soda-lime glass, which indicate a degree of non-volume-conserving deformation).

4.3. Dynamic fatigue measurements

An indentation load of 10 N was chosen for all three materials for the fatigue tests, corresponding to a range of ratios of initial crack size to minor phase grain size from 6.5 (SP(398)) to 2 (SP2(405)). At this indentation load the inert strength deviates slightly from ideal behavior (Fig. 3) and K_c is slightly smaller than that in the well-behaved region (Table 3). The dynamic fatigue plots obtained for these identically indented specimens are shown in Fig. 5. Regressions were performed on the data in order to obtain the parameters n' and λ' described by eqn. (6). Usage of the parameters σ_m and c_m obtained at $P = 10$ N and eqns. (7) and (8) then allowed the "true" fatigue parameters n and v_0 to be determined

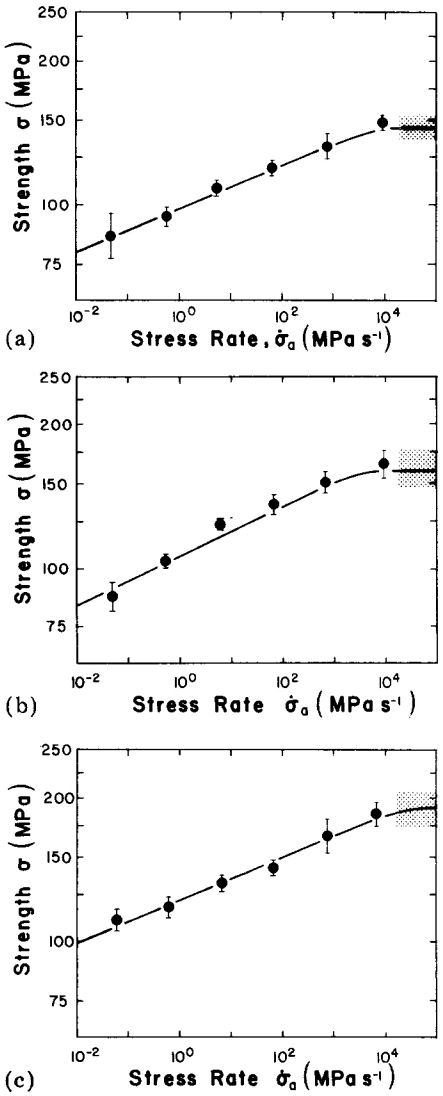

Fig. 5. Dynamic fatigue plots for the three materials (a) SP(398), (b) S(396) and (c) SP2(405) for contact loads of $P = 10$ N: ●, mean and standard deviation of seven to ten measurements at each stress rate; ——, numerical regeneration of the data using eqns. (7) and (8); the shaded band on the right-hand side represents the inert strength.

TABLE 4

Crack growth parameters

Material	n	$\log v_0$ (m s^{-1})	$\log \lambda'$
SP(398)	27.1 ± 2.6	−1.41 ± 0.13	43.4
S(396)	23.5 ± 2.3	−1.87 ± 0.14	38.8
SP2(405)	27.2 ± 2.7	−1.00 ± 0.14	45.7
Soda-lime glass	18.4	−1.50	—
Pyroceram C9606	116	5.0	—

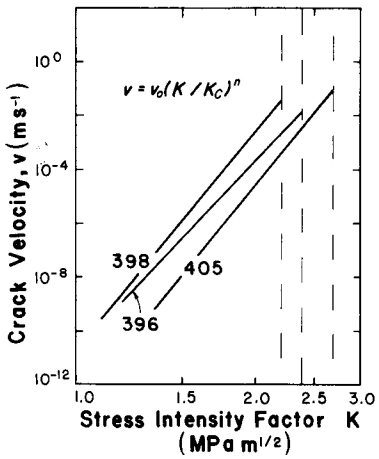

Fig. 6. Predicted $v(K)$ response of the three glass ceramics appropriate to the $P = 10$ N fatigue data. The similar susceptibilities to fatigue of the three glass ceramics can be seen in the slopes of the curves of this plot.

(Table 4). Using these data the fatigue curves were then regenerated numerically, these regenerated data are shown as the full lines in Fig. 5 [7]. The regenerated curves pass through all the fatigue data and then level off to the inert strength plateaus represented by the shaded bands, indicating that the transformation equations, eqns. (7) and (8), adequately describe the data, at least for single indentation loads. $v(K)$ curves were generated from the values of v_0, n and K_c obtained from the 10 N data (Fig. 6). The extent of the lines was determined from the range of stress intensity factors sampled by the fatigue tests. The results shown in Fig. 6 and Table 4 indicate that the fatigue susceptibility n is not significantly different for the three materials.

5. LIFETIME PREDICTIONS

5.1. Theory

The dynamic fatigue and inert strength data presented in Section 4 provide the basis for predicting component lifetimes under constant applied stress. Solution of the differential equation for the static fatigue condition, constant applied stress $\sigma_A (< \sigma_m)$, leads to an expression for the failure time [8]:

$$t_f = \left(\frac{\lambda'}{n'+1}\right)\sigma_A^{-n'} \qquad (9)$$

The above expression allows the prediction of lifetimes for components which have the same inert strength as those used in the dynamic fatigue tests. Frequently, however, lifetime predictions are required for components which have different inert strength levels from those used in determining the fatigue characteristics. Recent work in this area has used the stratagem of incorporating the contact load directly into the fatigue equations by noting that the parameter

$$\lambda'_P = \lambda' P^{(n'-2)/3} \tag{10}$$

is a material constant independent of P [12, 13]. However, the usage of this parameter and technique depends on the constancy of $\sigma_m P^{1/3}$. Since $\sigma_m P^{1/3}$ is not a constant for the materials studied here, we must resort to the stratagem of determining "effective" indentation loads to make valid lifetime predictions for different contact loads and hence different inert strength levels [13]. The general problem is to calculate λ' in eqn. (9) for different inert strength levels without relying on the $P^{-1/3}$ variation in the inert strengths.

We begin by noting that eqn. (10) allows us to write

$$\lambda'_2 = \lambda'_1 \left(\frac{P_1}{P_2}\right)^{(n'-2)/3} \tag{11}$$

where P_2 and P_1 are indentation loads and λ'_2 and λ'_1 their corresponding fatigue parameters. We know that eqn. (11) will not be valid here if the actual indentation loads are used (since $\sigma_m P^{1/3}$ is not constant). However, we may avoid the explicit use of indentation loads by generating their *effective ratio*. This is derived from eqn. (4) such that the ratio is consistent with the measured inert strengths:

$$\frac{P_1}{P_2} = \left(\frac{\sigma_2}{\sigma_1}\right)^3$$

where σ_2 and σ_1 are the inert strengths in question. By generating these "apparent" or "effective" indentation loads from the inert strengths we are able to use the techniques of the previous studies [13]. Thus, combining this equation and eqn. (11), we may generate failure time parameters λ'_{σ_2} for any inert strength level σ_2:

$$\lambda'_{\sigma_2} = \lambda'_1 \left(\frac{\sigma_2}{\sigma_1}\right)^{n'-2} \tag{12}$$

from a measured parameter λ'_1 corresponding to a measured inert strength of σ_1. Provided that the value of n' does not change, this equation will provide the correct relationship between failure time parameters and the inert strengths. This is because apparent toughness characteristics as described by inert strength–indentation load data do not enter the equation. Figure 7 shows the errors in lifetime prediction that occur when the value of λ' is wrongly calculated. The quantity t_f/t_f' representing the actual component lifetime for a given inert strength divided by the lifetime predicted on the basis of indentation load is simply equal to the ratio $\lambda'_{\sigma_2}/\lambda'_2$. The parameter λ'_{σ_2} was calculated from eqn. (12) using the inert strength data of Fig. 4 and λ'_2 was calculated from eqn. (11) using the indentation loads. (The reference value λ'_1 was the $P = 10$ N value taken from the experimental fatigue data.) The quantity t_f/t_f' is less than unity for indentation loads less than the reference level, indicating that lifetimes will be overestimated in this region, the tendency increasing for increasing grain size. It should be strongly emphasized that this is not a trivial effect as overestimates of two orders of magnitude could occur for the SP2(405) material just over the range of indentation loads tested here. Equation (12) may be used to generate dynamic fatigue curves in combination with eqn. (6) for any inert strength level or in combination with eqn. (9) for static fatigue curves. By using the latter method we gain

$$t_f = \frac{\lambda'_1 (\sigma_2/\sigma_1)^{n'-2}}{(n'+1)\sigma_A^{n'}} \tag{13}$$

5.2. *Predictions*

Equation (13) may be used in two different ways to predict component lifetimes. The first of these is to set the level of the inert strength of the components in question (σ_2 above). Then by incorporation of the values of σ_1, n' and λ'_1 obtained from dynamic fatigue experiments on the materials under examination, component lifetimes may be generated for various applied stress levels. This technique is demonstrated in Figs. 8(a) and 8(b) which show lifetime predictions for the SP(398) and SP2(405) materials at (fictitious) inert strength levels of 100 MPa and 200 MPa (5% uncertainty

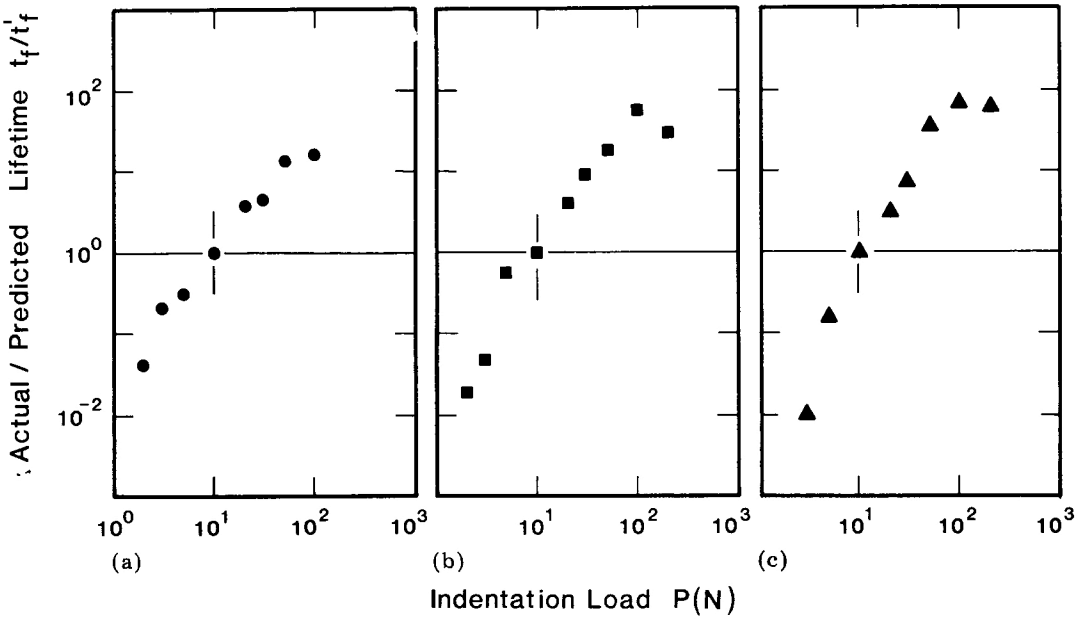

Fig. 7. Lifetime predicted on the basis of the observed inert strengths compared with that predicted from the contact load assuming constant toughness for the three materials (a) SP(398), (b) S(396) and (c) SP2(405). The reference load ($P = 10$ N) at which the fatigue data were measured is indicated by the vertical lines. Errors in lifetime prediction occur for contact loads other than the reference and this tendency increases with increasing grain size.

assumed in each). The hatched bands represent standard deviations of the lifetimes, calculated by error propagation methods. The center lines in each band are parallel, representing eqn. (13) and the degree of uncertainty in lifetime increases with decreasing applied stress or increasing failure time. On the basis of these predictions there is little to decide between these materials, as their fatigue characteristics are very similar and toughness characteristics do not enter eqn. (13).

The second method is to set the peak contact load encountered by the components (*e.g.* during machining and finishing or subsequent in-service conditions). The corresponding inert strengths are then set by the effective toughness at that contact load. Accordingly, Figs. 8(c) and 8(d) show lifetime predictions for components of SP(398) and SP2(405) materials with the inert strengths taken from Fig. 3 appropriate to peak contact loads of 50 and 3 N. Two important differences now appear between the predictions for the two materials. First, the lifetimes of the SP2(405) material are greater for the same applied stress, particularly at the 50 N level. This corresponds to the greater average toughness of this material (Fig. 4). Secondly the separation of the 50 and 3 N level lifetimes is smaller for the SP2(405) material. This effect is due to the greater departure in inert strength from the $P^{-1/3}$ dependence for this material, as shown in Fig. 3.

Microstructural influences on lifetime predictions thus appear only when peak contact loads (as opposed to the inert strengths) are specified, as may be seen by comparing Fig. 8(a) with 8(b) and Fig. 8(c) with 8(d), as then toughness characteristics are implicitly incorporated in eqn. (13).

6. DISCUSSION

6.1. Strength and toughness variations

The greater resistance to crack propagation as measured by its larger fracture toughness appears to make the large-grain-size SP2(405) material the best choice for structural applications. The greater toughness of this material is seen in both the value measured in the well-behaved large-contact-load and large-flaw-size region of the data (Table 3) and in the average values taken from the range of flaw sizes tested (Figs. 2 and 4). The greater magnitude

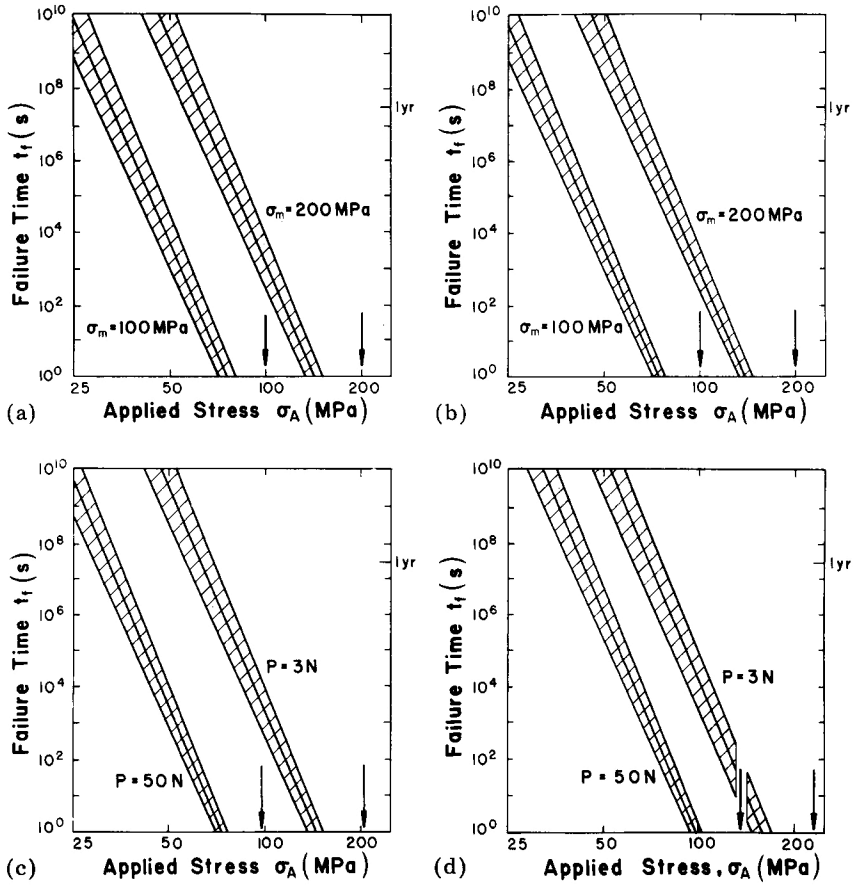

Fig. 8. Lifetime predictions at a constant applied stress for components of the (a), (c) SP(398) and (b), (d) SP2(405) materials for (a), (b) assumed initial strengths of 100 and 200 MPa and (c), (d) assumed contact loads of 3 and 50 N. The center line in each band represents the prediction of eqn. (13) and the width of the band represents the standard deviation in the lifetime at the applied stress; the vertical arrows represent the appropriate inert strength.

of the toughness appropriate to large flaws implies that this material would be more able to resist the propagation of large macroscopic cracks driven solely by remote applied stresses. The greater effective toughness averaged over the range of contact flaws tested suggests that the SP2(405) material will also be more resistant to failure from contact events. The larger "effective" contact toughness is reflected in the increased predicted lifetimes for this material as shown in Figs. 8(c) and 8(d).

Increases in fracture toughness with increasing grain size as observed in the series SP(398), S(396), SP2(405) have been observed in a number of materials [14–16]. One explanation is that, at large grain sizes, greater crack deflection occurs as the crack preferentially traverses the weaker less tough phase or grain boundary, causing more mechanical energy to be used for the same crack extension [16]. Indeed Faber and Evans [17] in their recent work on SiC suggest that high aspect ratio additions would produce the kind of toughening behavior experimentally found in this study and in work on Ba_2SiO_4 glass ceramics [18, 19].

If crack deflection influences the effective toughness of these materials, we might expect K_c^{eff} and hence the inert strength to vary with the ratio of the crack length to the mean free path in a component. As a crude test of this, Fig. 9 shows the inert strengths of the materials plotted as a function of the ratio c_0'/λ of the initial crack size to the mean free path. The strength data for all three materials now lie on a single curve. At large crack sizes the strengths

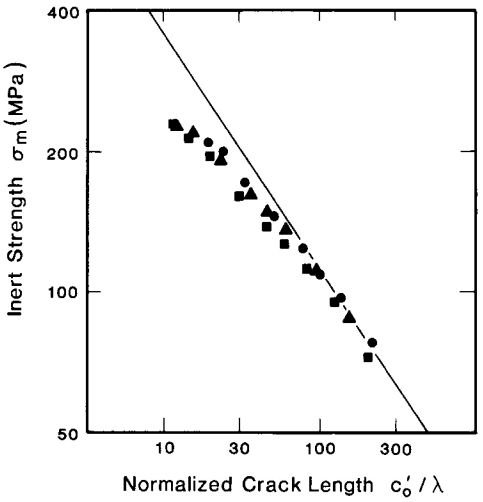

Fig. 9. Strength degradation plot showing the deviation from the expected $c^{-1/2}$ dependence at small crack sizes: ●, SP(398); ■, S(396); ▲, SP2(405). Plotted against the initial crack length normalized by the mean free path, the strength data fall on a single curve for all three materials.

tend to the usual $c^{-1/2}$ relation (full line). However, at small crack sizes (compared with the scale of the microstructure) the strengths deviate strongly from the line, the deviations occurring with approximately the same dependence on c_0'/λ for all three materials. Arbitrary as this approach may be, it shows that it is not only the absolute scale of the microstructure which influences strength but also the scale relative to the dominant flaw size. Observations of indentation cracks in these materials showed that they were not totally deflected by the minor phase particles, a phenomenon observed in similar glass ceramics [16]. However, the evidence of Fig. 9 and comparisons of the effective fracture toughness of these two-phase materials with that (about 1.2 MPa $m^{1/2}$) of pure SiO_2 suggests that crack deflection is probably a toughness-controlling mechanism in this system.

Similar deviations from the model $P^{-1/3}$ (or $c^{-1/2}$) variations in indentation strength have recently been observed in a number of systems, Al_2O_3 [20], $BaTiO_3$ [21] and a cordierite glass ceramic [22]. The recent work of Lawn *et al.* [20] on Al_2O_3 has suggested that strengths at low contact loads should tend to plateaus inversely related to the scale of the microstructure, a phenomenon not observed here. This implies that other factors not necessarily scaling with the microstructure may also be influencing observed strengths. These include internal stresses produced by the thermal expansion anisotropy of the material or by volume changes occurring during crystallization [19, 21]. Microcracking has been observed in glass ceramics similar to these [16] and may also be an influencing factor, particularly at large crack sizes.

6.2. *Reliability predictions*

The assumption was made in predicting lifetimes for contact loads and inert strengths other than those used in the determination of the fatigue characteristics that the fatigue susceptibility was independent of the contact load. Experimental evidence for the validity of this assumption may be seen in Table 4; the n values determined for the three materials are seen to be negligibly different even though different ratios of starting flaw size to microstructure size were used for each material. It can be argued that, since the n value was independent of this ratio for the different materials, it will be independent of this ratio for the same material. Recent dynamic fatigue data on Al_2O_3 and $BaTiO_3$ using different indentation loads have suggested that n is in fact invariant with respect to the ratio of the flaw size to the microstructure size [23]. In fact, if the stress-enhanced chemical reaction at the crack tip does not vary, then n and v_0 will be invariant as long as there is no transition from transgranular to intergranular crack growth or vice versa.

In reliability predictions it is generally the evaluation of n which is critical since uncertainty in the failure time largely arises from uncertainty in n. However, if microstructural influences are present in the material, systematic errors in lifetime prediction may occur. Figure 4 shows that the effective toughness values for small flaws for these materials may be only 70% of that determined using macroscopic cracks. As a consequence of this variation and the strong power law dependence of the fatigue parameter λ' on effective toughness, overestimates by factors of 10^4 in predicted lifetime may result if macroscopic $v(K)$ data are extrapolated to small flaw sizes (Fig. 7). Hence variations in K_c^{eff} with flaw size should be

well characterized for accurate lifetime predictions if extrapolation is required to different flaw sizes. The usefulness in choosing a high toughness material may disappear if only low contact loads are encountered in service. Careful inspection of Figs. 8(c) and 8(d) will reveal that there is little difference in the predicted lifetimes of the SP(398) and SP2(405) materials with peak contact loads of 3 N.

7. CONCLUSIONS

(1) Microstructural effects were evident in the inert strengths of the three materials studied as deviations from the well-established $P^{-1/3}$ dependence of strength on contact load. Deviations were most pronounced in the larger-grain-size materials and consisted of a decrease in strength below the expected line at low contact loads. The larger-grain-size materials also showed greater strengths for a given contact load, indicating an increase in toughness with grain size.

(2) The material SP2(405) is predicted to be the best choice as a structural ceramic on the basis of its greater overall effective toughness. However, the severe decrease in strength of the SP2(405) material means that there would be only a minor advantage in choosing this material if only low contact loads were encountered in service. All three materials showed approximately the same susceptibility to moisture-enhanced slow crack growth as characterized by the fatigue exponent n. Hence the variability in reliability predictions largely arose through variations in the apparent toughness.

(3) Lifetime prediction using the technique of incorporating the contact load explicitly into the reliability parameters is precluded in this case by the apparent toughness variations. However, predictions can still be made if inert strengths are used as the basis of lifetime prediction. If contact load is required as a design parameter, explicit strength *versus* contact load data are needed.

(4) The above data suggest that a third term involving the microstructure should be added to the stress intensity factor for indentation flaws. Future work should concentrate on formulating this microstructural stress intensity which should probably incorporate a crack deflection mechanism. In this way a dependence on both the absolute scale of the microstructure and the relative crack-to-microstructure ratio would be incorporated.

ACKNOWLEDGMENTS

The authors gratefully acknowledge discussions with B. R. Lawn on aspects of this work.

Funding was provided by an Australian Commonwealth Postgraduate Research Award (R.F.C.) and the U.S. Department of Energy under Contract 31-5422.

REFERENCES

1 D. B. Marshall and B. R. Lawn, *J. Mater. Sci., 14* (1979) 2001.
2 B. R. Lawn, A. G. Evans and D. B. Marshall, *J. Am. Ceram. Soc., 63* (1980) 574.
3 G. R. Anstis, P. Chantikul, B. R. Lawn and D. B. Marshall, *J. Am. Ceram. Soc., 64* (1981) 573.
4 P. Chantikul, G. R. Anstis, B. R. Lawn and D. B. Marshall, *J. Am. Ceram. Soc., 64* (1981) 539.
5 R. F. Cook and B. R. Lawn, *Commun. Am. Ceram. Soc., 66* (1983) 200.
6 R. F. Cook, unpublished work, 1984.
7 R. F. Cook, B. R. Lawn and G. R. Anstis, *J. Mater. Sci., 17* (1982) 1108.
8 E. R. Fuller, Jr., B. R. Lawn and R. F. Cook, *J. Am. Ceram. Soc., 66* (1983) 314.
9 J. J. Mecholsky, personal communication, 1984.
10 S. W. Freiman, in L. L. Hench and R. W. Gould (eds.), *Characterization of Ceramics*, Dekker, New York, 1971, p. 555.
11 R. F. Cook, B. R. Lawn, T. P. Dabbs and P. Chantikul, *Commun. Am. Ceram. Soc., 64* (1981) C121.
12 R. F. Cooke and B. R. Lawn, *ASTM Spec. Tech. Publ., 844* (1984) 22.
13 A. C. Gonzalez, H. Multhopp, R. F. Cook, B. R. Lawn and S. W. Freiman, *ASTM Spec. Tech. Publ., 844* (1984) 43.
14 R. W. Rice, S. W. Freiman and P. F. Becher, *J. Am. Ceram. Soc., 64* (1981) 345.
15 B. Mussler, M. V. Swain and N. Claussen, *J. Am. Ceram. Soc., 65* (1982) 566.
16 K. T. Faber and A. G. Evans, *Acta Metall., 31* (1983) 577.
17 K. T. Faber and A. G. Evans, *Commun. Am. Ceram. Soc., 66* (1983) C94.
18 S. W. Freiman, G. Y. Onoda, Jr., and A. G. Pincus, *J. Am. Ceram. Soc., 57* (1974) 8.
19 J. J. Mecholsky, in R. C. Bradt, A. G. Evans,

D. P. H. Hasselman and F. F. Lange (eds.), *Fracture Mechanics of Ceramics*, Vol. 6, Plenum, New York, 1983, p. 165.
20 B. R. Lawn, S. W. Freiman, T. L. Baker, D. D. Cobb and A. C. Gonzalez, *J. Am. Ceram. Soc.*, *67* (1984) C67.
21 R. F. Cook, S. W. Freiman, B. R. Lawn and R. C. Pohanka, *Ferroelectrics, 49* (1983) 593.
22 R. Morena, K. Nihara and D. P. H. Hasselman, *J. Am. Ceram. Soc.*, *66* (1983) 6773.
23 R. F. Cook, B. R. Lawn, S. W. Freiman and T. L. Baker, unpublished work, 1984.